Nonuniform Beamfilling Correction for Spaceborne Radar Rainfall Measurement: Implications from TOGA COARE Radar Data Analysis

TOSHIAKI KOZU AND TOSHIO IGUCHI

Communications Research Laboratory, Koganei, Tokyo, Japan

(Manuscript received 14 May 1998, in final form 27 October 1998)

ABSTRACT

A method is studied to make a nonuniform beamfilling (NUBF) correction for the path-integrated attenuation (PIA) derived from spaceborne radar measurement. The key of this method is to estimate rain-rate variability within a radar field of view from the local statistics of a radar-measurable quantity ($\langle Q \rangle$) such as PIA derived from the surface reference technique. Statistical analyses are made on spatial variabilities of the radar-measurable quantities using a shipborne radar dataset over the tropical Pacific obtained during the TOGA COARE field campaign. It is found that there are reasonably good correlations between the coarse-scale variability of $\langle Q \rangle$ and the finescale variability of rain rate, and the regression coefficient (slope) of these two quantities depends somewhat upon rain types. Based on the statistical analyses, the method is tested with a simulation using the same dataset. The test result indicates that this method is effective in reducing bias errors in the estimation of rain-rate statistics. Although it is also effective to make the NUBF correction on an individual instantaneous field-of-view basis, one must account for the variability of local rainfall statistical characteristics that may cause significant errors in the NUBF correction.

1. Introduction

It is well known that nonuniform beamfilling (NUBF) is a major error source in quantitative rainfall remote measurement with a spaceborne rain radar if the footprint size of the radar is comparable to or larger than a convective cell size. The effect of NUBF depends also upon the algorithm for estimating rain rate. It has been shown that the use of the path-integrated attenuation (PIA) derived from the surface return method [surface reference technique (SRT)] suffers more from the NUBF effect than the use of radar reflectivity factor with a Z–R relation for rain-rate estimation (Nakamura 1991; Amayenc et al. 1993). However, SRT is recognized as a very important method to achieve a quantitative retrieval of heavy rain (about 20 mm h^{-1} or higher) because it provides a reference to stabilize the rain attenuation correction that often becomes unstable if we know only a measured and attenuated Z-factor profile (Meneghini and Kozu 1990). It is therefore crucial to develop a method to judge the existence of significant NUBF (to issue a ''warning'' flag), and, if possible, to develop a method to correct the SRT-derived path attenuation for the NUBF effect. Since the attenuation coefficient (in dB per unit distance) has an approximately linear relationship with rain rate, obtaining accurate PIA is also useful to estimate path-integrated rain rate.

We have studied a method for correcting the SRT-measured PIA for the NUBF effect (Kozu and Iguchi 1996, 1997) and have shown that the method has a potential to reduce bias errors in PIA estimation based upon case studies using shipborne and ground-based radar data from the Tropical Ocean Global Atmosphere (TOGA) Coupled Ocean–Atmosphere Response Experiment (COARE) (Short et al. 1995). This method is based upon a characteristic of spatial variability of rain intensity, which has been used for the SSM/I rain-rate retrieval algorithm by Kummerow and Giglio (1994). They showed a fairly good correlation between the normalized standard deviations (NSDs) of rain at 1-km resolution and the NSD at 12.5-km resolution, the latter being obtained from the 85-GHz channel of SSM/I, and made an NUBF correction using the estimated 1-km resolution NSD. In the case of radar measurement, however, the spatial scale of interest is approximately equal to the correlation length of individual rain cells, which is much smaller than those of SSM/I. Therefore, we may find characteristics different from the result of Kummerow and Giglio (1994). Graves (1993) also pointed out that statistical properties of rain field tend to be unstable as the size of instantaneous field of view (IFOV) becomes small, making a statistical NUBF correction difficult in his statistical modeling of NUBF for microwave radiometer measurements of oceanic rainfall.

This paper, which is the result of a study following the

Corresponding author address: Dr. Toshiaki Kozu, Department of Electronic and Control Systems Engineering, Shimane University, 1060 Nishi-kawatsu Matsue, Shimane 690-8504, Japan.
E-mail: kozu@ecs.shimane-u.ac.jp

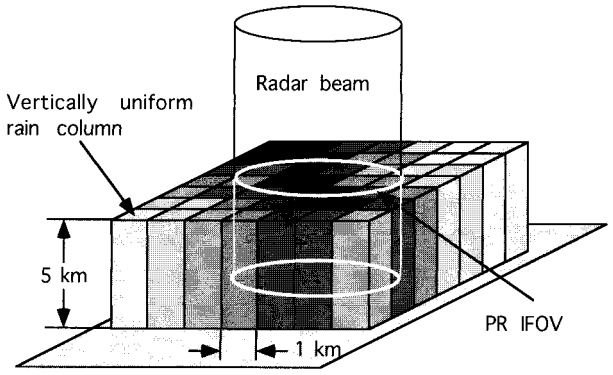

FIG. 1. Concept of storm model.

work of Kozu and Iguchi (1996, 1997), describes comprehensive statistical analyses of shipborne radar data obtained between November 1992 and February 1993 over the tropical Pacific. In the following sections, we describe 1) basic formulation of the problem, 2) the NUBF correction method, 3) statistical characteristics of rainfall, and 4) a simulation of the NUBF correction.

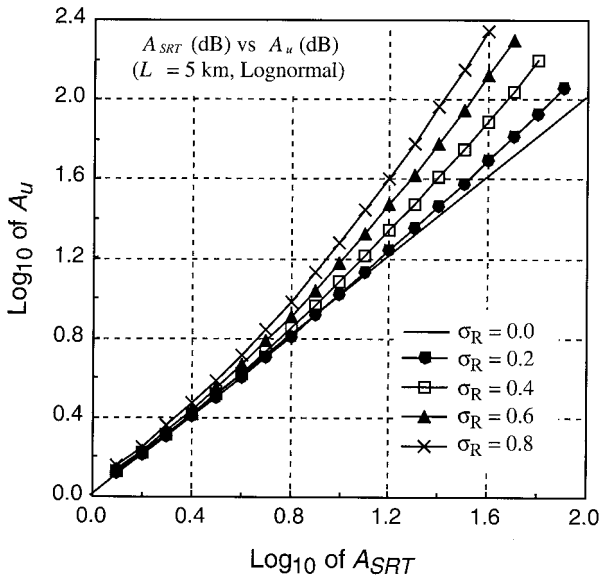

FIG. 2. Relationship between "uniform" PIA (A_u) and SRT-derived PIA (A_{SRT}) assuming the lognormal PDF and a rain depth L of 5 km as the normalized standard deviation of rain rate (σ_R) as a parameter.

2. Rain and observation models

a. PDF and its parameters

We assume a vertically uniform, horizontally nonuniform rain model in an IFOV as shown in Fig. 1. This model is valid when we consider the SRT because it deals with only the path-integrated values. In this situation, we assume that we can measure a PIA with the SRT, a storm height, and a Z-factor profile that includes propagation loss due to rain.

If we assume that the probability density function (PDF) of rain rate in the IFOV is approximated by a lognormal model with the expectation of R, $\overline{R}$, and the NSD of R, σ_R (i.e., we assume "uniform" statistics within the IFOV), then the PDF, $f(R)$, is expressed as

$$f(R) = \frac{1}{\sqrt{2\pi}\xi_R R}\exp\left[-\frac{(\ln R - \mu_R)^2}{2\xi_R^2}\right], \qquad (1)$$

where μ_R and ξ_R^2 are the mean and the variance of $\ln R$, which are related to $\overline{R}$ and σ_R as follows:

$$\overline{R} = \exp(\mu_R + \xi_R^2/2), \qquad \sigma_R^2 = \exp\xi_R^2 - 1. \qquad (2)$$

With this expression, the PIA measured with the SRT, A_{SRT}, in decibels, is given by

$$A_{\mathrm{SRT}} = -10\log\left\{\int_0^\infty \exp\left[-\frac{\ln 10}{10}A(R)\right]f(R)\,dR\right\} \qquad (3)$$

with

$$A(R) = 2LaR^b, \qquad (4)$$

where L is the storm depth, and a and b are the coefficient and exponent of the k–R relation (attenuation coefficient versus rain-rate relation). We define the uniform PIA, A_u, as the PIA that corresponds to $\overline{R}$ with a usual k–R relation that can be obtained when rain is uniform within the IFOV:

$$A_u = 2La\overline{R}^b. \qquad (5)$$

Using $\overline{R}$ and σ_R as parameters, we can relate A_{SRT} to A_u. The relationship between those quantities assuming the lognormal PDF and a rain depth L of 5 km is shown in Fig. 2.

Since k–R and Z–R relations are generally expressed as power laws,

$$k = aR^b \quad \text{and} \quad Z = \alpha R^\beta, \qquad (6)$$

the distributions of k and Z are also lognormal and the means and variances of $\ln k$ (μ_k, ξ_k^2) and those of $\ln Z$ (μ_Z, ξ_Z^2) are given by

$$\mu_k = \ln a + b\mu, \qquad \xi_k^2 = b^2\xi_R^2, \qquad (7)$$

$$\mu_Z = \ln\alpha + \beta\mu, \qquad \xi_Z^2 = \beta^2\xi_R^2. \qquad (8)$$

Thus, the expectation and NSD of k ($\overline{k}$, σ_k) and those of Z ($\overline{Z}$, σ_Z) are expressed as

$$\overline{k} = \exp(\mu_k + \xi_k^2/2) = a\overline{R}^b\exp[b(b-1)\xi_R^2], \qquad (9)$$

$$\sigma_k^2 = \exp\xi_k^2 - 1 = (\sigma_R^2 + 1)^{b^2} - 1, \qquad (10)$$

$$\overline{Z} = \exp(\mu_Z + \xi_Z^2/2) = \alpha\overline{R}^\beta\exp[\beta(\beta-1)\xi_R^2], \quad \text{and} \qquad (11)$$

$$\sigma_Z^2 = \exp\xi_Z^2 - 1 = (\sigma_R^2 + 1)^{\beta^2} - 1. \qquad (12)$$

Equations (10) and (12) indicate that NSDs of k and Z are different from the NSD of rain rate but can easily

be converted. Please note that the parameter σ_R in Fig. 2 is the NSD of rain rate (not of attenuation coefficient). In the calculation of A_u and A_{SRT}, the difference in PDF parameters is incorporated.

b. Relation between point and area-averaged quantities

Before describing the NUBF correction method, we consider the relationship between a ''point'' quantity Q and an ''area-averaged'' counterpart $\langle Q\rangle$ that is a basis of the current method. A similar problem has been discussed in the study of methods to predict PIA from a point measurement of rain rate with a rain gauge (Morita and Higuti 1978). They derived expressions for the mean and variance of PIA using a ''normalized spatial autocorrelation function'' (hereafter, ACF) of rain rate expressed by the form of $\exp(-\zeta\sqrt{r})$, where r is the distance between two points. In this paper, we derive an expression of Q (vertically averaged or integrated quantity with high spatial resolution) and $\langle Q\rangle$ (area-averaged value of Q over the IFOV). Note that the difference between the notation $\overline{Q}$ and $\langle Q\rangle$ is that the former is the expectation and the latter is still a statistical random variable.

First, we assume the following ACF model that depends on distance only:

$$\rho(r) = \exp(-\zeta r^{\eta}), \tag{13}$$

where r is the distance between two points on a two-dimensional rain field. As we see later in this paper, this model can well fit the ''averaged'' 1D ACF that is generated from the observed 2D ACF by making an ''isorange'' circular averaging. Of course, there may be a wide range of directional properties in the 2D ACF, depending on storm type and orientation. Nevertheless, the approximation used here would be useful to obtain approximate properties of the relation between NSDs in connection to the ACF of rain field. Let $Q(x, y)$ be the point value at (x, y) and $\langle Q(x_0, y_0)\rangle$ be the spatially averaged Q over a circular area having the diameter D centered at (x_0, y_0). In addition, let $\overline{Q}$ and σ'_Q be the mean and NSD of Q. We add $(')$ to σ_Q because we implicitly assume here that rain-rate fluctuations having any spatial frequency can contribute to the variability of Q, which may be different from the variability of Q within an IFOV. Then we have the following relations:

$$\overline{\langle Q\rangle} = \overline{Q}, \qquad \sigma^2_{\langle Q\rangle} = \{\overline{\langle Q\rangle^2} - \overline{Q}^2\}/\overline{Q}^2. \tag{14}$$

If we assume that $\rho(r)$ is independent of the location (x, y), $\{\overline{\langle Q\rangle^2} - \overline{Q}^2\}$ can be written as

$$\begin{aligned}
\overline{\langle Q\rangle^2} - \overline{Q}^2 &= \frac{16}{\pi^2 D^4}\int\!\!\int_{x_2,y_2}\int\!\!\int_{x_1,y_1}\overline{Q(x_1, y_1)Q(x_2, y_2)}\,dx_1\,dy_1\,dx_2\,dy_2 - \overline{Q}^2,\\
&= \frac{16}{\pi^2 D^4}\int\!\!\int_{x_2,y_2}\int\!\!\int_{x_1,y_1}[\overline{Q}^2\sigma'^2_Q\rho(r) + \overline{Q}^2]\,dx_1\,dy_1\,dx_2\,dy_2 - \overline{Q}^2,\\
&= \frac{16\overline{Q}^2\sigma'^2_Q}{\pi^2 D^4}\int\!\!\int_{\theta_2,r_2}\int\!\!\int_{\theta_1,r_1}\rho(r_1)r_1\,dr_1\,d\theta_1 r_2\,dr_2\,d\theta_2,\\
&= \frac{16\overline{Q}^2\sigma'^2_Q}{\pi^2 D^4}\int_0^{2\pi}\int_0^{D/2}\int_0^{2\pi}\int_0^{Rm(\theta_1,r_2)} r_1\exp(-\zeta r_1^{\eta})\,dr_1\,d\theta_1 r_2\,dr_2\,d\theta_2,\\
&= \frac{32\overline{Q}^2\sigma'^2_Q\Gamma(2/\eta)}{\pi D^4\eta\zeta^{2/\eta}}\int_0^{D/2}\int_0^{2\pi}P(2/\eta,\ \zeta R_m^{\eta}(\theta_1, r_2))\,d\theta_1 r_2\,dr_2, \quad \text{and}\\
&= \frac{32\Gamma(2/\eta)}{\pi D^4\eta\zeta^{2/\eta}}B(D,\ \zeta,\ \eta)\overline{Q}^2\sigma'^2_Q,
\end{aligned} \tag{15}$$

where $P(\lambda, z)$ is the incomplete gamma function, and the double integral over θ_1 and r_2 is represented by a function $B(D, \zeta, \eta)$. Note that the above 2D integration is made over the circular region having a diameter D. A point $p(r_2, \theta_2)$ is first specified in the circle. The variable θ_1 is a polar angle about $p(r_2, \theta_2)$, and r_1 is defined as a distance from $p(r_2, \theta_2)$ to the edge of the circle in the direction of θ_1. Thus the upper limit of the integration over r_1 (R_m) is a function of θ_1 and r_2. Thus, the relation between σ'^2_Q and $\sigma^2_{\langle Q\rangle}$ can be expressed as

$$\begin{aligned}
\sigma^2_{\langle Q\rangle} &= \{\overline{\langle Q\rangle^2} - \overline{Q}^2\}/\overline{Q}^2\\
&= \frac{32\Gamma(2/\eta)}{\pi D^4\eta\zeta^{2/\eta}}B(D,\ \zeta,\ \eta)\sigma'^2_Q,
\end{aligned} \tag{16}$$

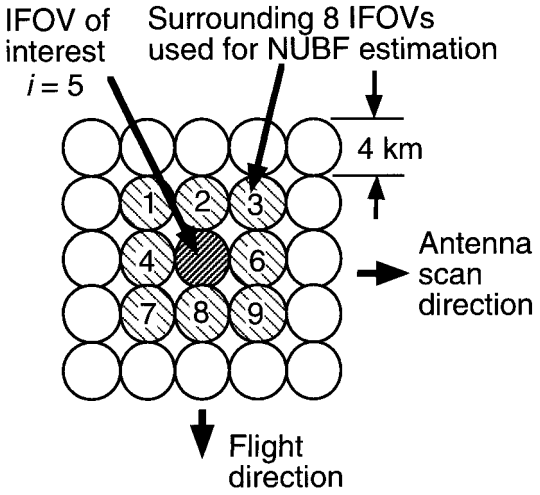

FIG. 3. Concept of down-looking rain radar IFOV used in the NUBF correction scheme.

which can be used to predict $\sigma_Q'^2$ from $\sigma^2_{\langle Q\rangle}$ and the parameters of the spatial correlation function, although a 2D integration is needed to evaluate $B(D, \zeta, \eta)$. It should be noted that the PDF form has nothing to do with Eq. (16), but the PDF does affect the correction factor to estimate A_u (see Fig. 2).

The difference between σ_Q and σ_Q' would be small when the diameter of IFOV is much wider than the correlation length of the ACF, which may be applicable for most spaceborne radiometers; however, this may not be the case for the 4-km IFOV we consider here. We will discuss this problem later in the discussion of the result of observation data analyses.

3. Description of correction method

As we discussed earlier, our final goal is to estimate A_u from radar-measurable quantities. The first step is to estimate parameters of the rain-rate PDF within an IFOV of interest, specifically $\overline{R}$ and σ_R. In this section we describe formulations using measurable quantities but do not include measurement errors to simplify the problem. The mean and NSD in this section represent the sample mean and sample NSD, respectively, which is different from the formulations in section 2, where we considered hypothetical random rain field with parent PDFs. To avoid a confusion, we denote a sample NSD "$\hat{\sigma}$," while the true NSD "σ" as was used in section 2.

Since we cannot directly measure $\langle R\rangle$, we cannot apply the direct relations connecting PDF parameters [Eqs. (2), (7)–(12)]; however, a quantity $\langle Q\rangle$ we can measure such as $A_{\rm SRT}$ would serve a proxy of $\langle R\rangle$ to estimate the NSD of R. To obtain an estimate of $\sigma\langle Q\rangle$, we use data at nine IFOVs (eight surrounding IFOVs and the IFOV at which we want to estimate σ_R), as shown in Fig. 3, which illustrates the geometry of spaceborne radar IFOVs related to this problem. Specifically, we estimate σ_R from SRT-derived PIA, $A_{\rm SRT}$. Although $A_{\rm SRT}$ is not proportional to $\langle k\rangle$, we will use this as a radar-measurable quantity. In the following, we formulate a discrete-model relationship for actual observation conditions, which can also be used for the simulation we discuss later.

Let $\langle R\rangle_i$ (i = 1–9) be the IFOV-averaged path-averaged rain rate, which consists of n rain-rate elements ($R_{j,i}$, $j = 1, n$) within the IFOV:

$$\langle R\rangle_i = \frac{\sum_{j=1}^{n} w_j R_{i,j}}{\sum_{j=1}^{n} w_j}, \tag{17}$$

where w_j is the weighting function representing the two-way antenna pattern. The PIA we should obtain when the rain is uniform in the IFOV, $A_{u,i}$ (dB), is

$$A_{u,i} = 2La\langle R\rangle_i^b \approx 2La'\langle R\rangle_i. \tag{5'}$$

The exponent b depends upon the frequency and drop size distribution, but it is fairly close to unity for the frequency range of interest (10–35 GHz) (Olsen et al. 1978). The last approximate equality in Eq. (5′) [see also Eq. (5)] represents this fact with a slight modification of the coefficient a to a' to get the best fit. Therefore, the NSD of PIA is generally close to that of path-averaged rain rate, and the $A_{\rm SRT}$–A_u relationship derived for a specific rain depth can be used for different rain depth cases. In other words, the variation of rain depth is not a problem if the rain rate averaged over a given rain depth follows the same type of PDF form as that assumed to generate the $A_{\rm SRT}$–A_u relationship. Note that the "given" rain depth should be equal to or higher than the maximum rain depth of interest.

Similar to $R_{j,i}$, the PIA element $A_{j,i}$ is expressed as

$$A_{j,i} = 2Lk_j = 2LaR_{j,i}^b \approx 2La'R_{j,i}. \tag{18}$$

The SRT-measured PIA ($A_{\rm SRT}$) is given by

$$A_{{\rm SRT},i} = -10\log\left[\frac{1}{\sum_{j=1}^{n} w_j}\sum_{j=1}^{n} w_j \exp(-0.2L\ \ln 10 aR_{j,i}^b)\right]. \tag{19}$$

The sample NSD of rain rate within the ith IFOV ($\hat{\sigma}_{R,i}$) is given by

$$\hat{\sigma}_{R,i} = \frac{\left[\dfrac{1}{\sum_{j=1}^{n} w_j}\sum_{j=1}^{n} w_j(R_{j,i} - \langle R\rangle_i)^2\right]^{1/2}}{\langle R\rangle_i}. \tag{20}$$

As an estimate of NSD in a coarse spatial-scale rain field ($\sigma_{\langle Q\rangle}$), we use the nine samples of a radar-measurable quantity, $\langle Q\rangle$:

TABLE 1. Summary of rain scenes used for the current study. For example, 921112_0301 represents 0301 UTC 12 Nov 1992.

Type 1 Squall line	Type 2 Randomly spread convective	Type 3 Widespread stratiform	Type 4 Widespread convective/stratiform
921112_0301	921111_0101	921111_0301	921224_1102
921124_1502	921122_1305	921126_2202	921124_1902
921220_0503	921220_0911	921220_1702	930117_1402
921222_0302	921224_0502	921222_0402	930130_1701
921229_1002	921224_1002	921224_1502	930210_0404
930103_0801	921226_0502	930117_1701	
930107_0102	930129_2212	930211_1802	
930110_0002	930103_1802	930215_1701	
930130_0002	930117_1002	930219_1702	
930209_1102	930131_0701	930223_1902	
930211_1402	930210_0301		
930212_0902	930219_1301		
930215_0601	930223_1601		
930218_2001			

$$\hat{\sigma}_{\langle Q\rangle} = \frac{\left[\frac{1}{9}\sum_{i=1}^{9}(\langle Q\rangle_i - \overline{\langle Q\rangle})^2\right]^{1/2}}{\overline{\langle Q\rangle}}, \qquad (21)$$

where $\overline{\langle Q\rangle}$ is the average of $\langle Q\rangle_1$–$\langle Q\rangle_9$.

As the radar-measurable quantity, we will use the PIA measured with the SRT (A_{SRT}). In the procedure for correcting A_{SRT}, the coarse-resolution NSD, $\hat{\sigma}_{A\mathrm{SRT}}$, is first obtained from the measured A_{SRT}, where $\hat{\sigma}_{A\mathrm{SRT}}$ represents $\hat{\sigma}_{\langle Q\rangle}$ when $\langle Q\rangle = A_{\mathrm{SRT}}$. Next, $\sigma_{R,5}$ is estimated from $\hat{\sigma}_{A\mathrm{SRT}}$ using a statistical relation (regression result) between $\hat{\sigma}_{A\mathrm{SRT}}$ and $\hat{\sigma}_R$ (which will be described later). Finally, $A_{u,5}$ is estimated from $A_{\mathrm{SRT},5}$ and $\sigma_{R,5}$ using the relation between A_{SRT} and A_u for a given σ_R assuming a lognormal PDF within the IFOV. In this case, the bias error in the sample NSD ($\hat{\sigma}_R$) is neglected because the bias error in the $\hat{\sigma}_R$–$\hat{\sigma}_{A\mathrm{SRT}}$ relationship is expected to be very small (≈2%) and will be masked by other error sources.

4. Statistical characteristics of rainfall over tropical Pacific

a. Data source

To study the rainfall characteristics statistically, we use 42 constant-altitude plan position indicator (CAPPI) maps at 2-km altitude obtained from the Massachusetts Institute of Technology (MIT) radar on board the R/V *Vickers* during the TOGA COARE campaign from November 1992 to February 1993. Those rain scenes are listed in Table 1 with a ''subjective'' rain-type classification. Though subjective, the classification may be useful to get approximate information about the rain-type dependence of the statistical characteristics. Examples of CAPPI data for types 1–4 are shown in Fig. 4. Please note that the classification is based on the characteristics of the area having a radius of 40 km centered at the radar location. The parameters to process the CAPPI *Z*-factor maps are listed in Table 2.

b. Spatial correlation properties of rain rate

As we discussed in section 3, the relation of variabilities between ''point'' rainfall quantity (Q) and area-averaged ($\langle Q\rangle$) quantity can be estimated if we know the parameters of the ACF of Q, and the averaging area (represented by D). This is approximately true when we relate R and $\langle Q\rangle$, where Q is not necessarily equal to R. In other words, characterizing the ACF of R would be useful to estimate the σ'_R–$\sigma_{\langle Q\rangle}$ relationship. For this purpose, we calculate the 2D ACF of rain rate. This is then averaged over an isorange circle so that we can obtain an averaged 1D ACF. Examples of the averaged 1D ACF are shown in Fig. 5 as well as the fitting with the model function of Eq. (13). The calculation of the 2D ACF is made over two regions on a CAPPI scene; 64 km by 64 km squares to the left and right of the radar site. This is because there is always a ''blind'' region near the radar site and sometimes to the north or south of the radar as well. It is found that Eq. (13) provides an excellent fit to the ACFs for almost all cases. Figure 6 shows the histograms of the averaged 1D ACF parameters ζ and η. On average, $\zeta \approx 0.135$ and $\eta \approx 1.13$ for convective types (types 1, 2, and 4) and $\zeta \approx 0.064$ and $\eta \approx 1.10$ for the stratiform type (type 3). Using Eq. (16) with $D = 4$ km, the relation between $\sigma_{\langle R\rangle}$ and σ'_R can be obtained.

As we discussed in the last paragraph of section 2, however, we need to consider the effect of 4-km windowing to convert σ'_R to the windowed NSD, σ_R. A theoretically rigorous treatment of this problem is beyond the scope of this paper; in the following, we consider this problem intuitively. Random rain-rate fluctuations, in which wavelengths are less than 4 km, clearly contribute to the variability of rain rate in a 4-km IFOV. The contribution of a fluctuation with spatial wavelength (λ) to σ_R decreases when λ becomes longer. A simple simulation evaluating the reduction factor versus λ has indicated that the contribution is reduced to about 70% when $\lambda = 8$ km. Thus, we assume the following approximate relation:

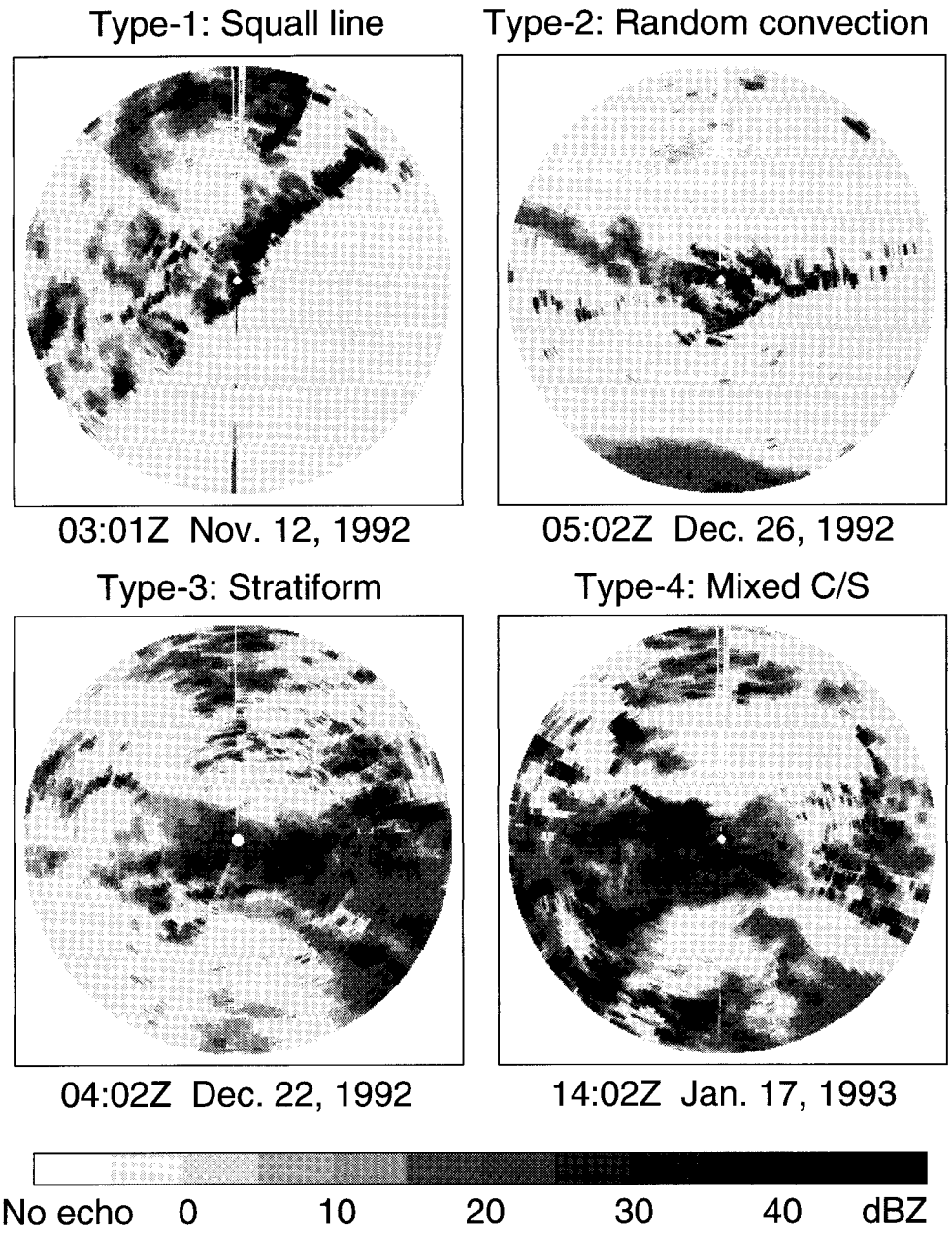

FIG. 4. Example of MIT radar 2-km CAPPI images (radius = 150 km). Note that only the 80 km by 80 km square area centered at the radar site is used for the NUBF study.

TABLE 2. Parameters for the analysis of MIT radar data.

Item	Specification
Data source	2-km CAPPI of the MIT radar on board *Vickers* in TOGA COARE
Processed data area	80 km × 80 km square, centered at the ship (for $\sigma_R - \sigma_{\langle Q \rangle}$ relation and simulation) 64 km × 64 km squares left and right of the ship (for spatial correlation function)
Z–R relation	$Z = 234R^{1.59}$
k–R relation	$k = 0.0237R^{1.17}$
Rain column height	5 km, vertically uniform (2-km CAPPI data are used throughout the 5-km column)
Rain-rate PDF model	Lognormal

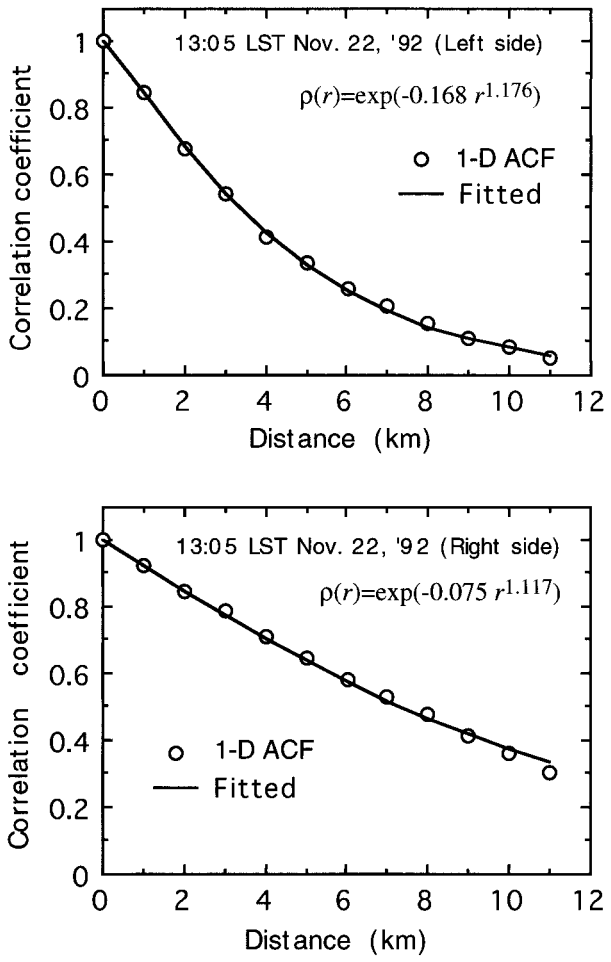

FIG. 5. Example of the averaged 1D ACF of rain rate.

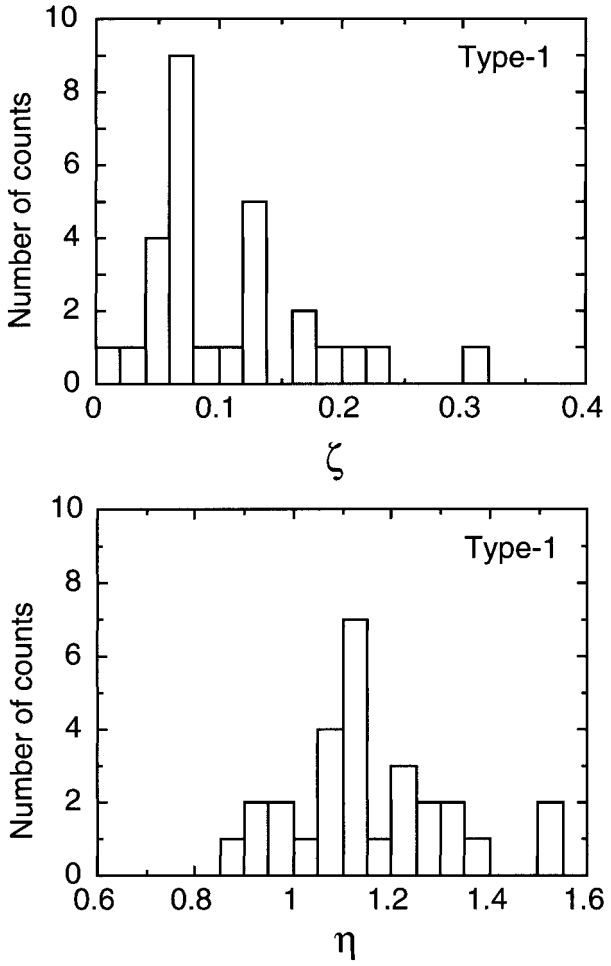

FIG. 6. Histograms of parameters of the averaged 1D ACF $\rho(r) = \exp(-\zeta r^{\eta})$ for rain type 1. The parameters are obtained for the left and right sides of each rain scene.

$$\sigma_R \approx [\sigma_R'^2 - \sigma^2_{\langle R\rangle(D=8\text{ km})}]^{1/2}, \tag{22}$$

where $\sigma^2_{\langle R\rangle(D=8\text{ km})}$ represents the $\sigma^2_{\langle R\rangle}$ with an IFOV diameter of 8 km. Using Eq. (16), the coefficient $c_{\langle R\rangle}$ relating $\sigma_{\langle R\rangle}$ to σ_R,

$$\sigma_R = c_{\langle R\rangle}\sigma_{\langle R\rangle}, \tag{23}$$

can be calculated and is shown in Fig. 7. It is found that $c_{\langle R\rangle}$ is about 0.72. For $\zeta \approx 0.135$ and $\eta \approx 1.13$ (mean values for convective rains), $c_{\langle R\rangle}$ is about 0.66. Equation (23) can be generalized as follows to estimate σ_R from any $\langle Q\rangle$:

$$\sigma_R = c_{\langle Q\rangle}\sigma_{\langle Q\rangle}. \tag{23a}$$

Note that Eqs. (23) and (23a) will also be used to relate sample NSDs (i.e., $\hat{\sigma}_R = c_{\langle Q\rangle}\hat{\sigma}_{\langle Q\rangle}$) as an approximate sense.

c. *Relation between finescale and coarse-scale rainfall variabilities*

The relation Eq. (23a) can also be obtained directly from actual radar data by a regression analysis, although

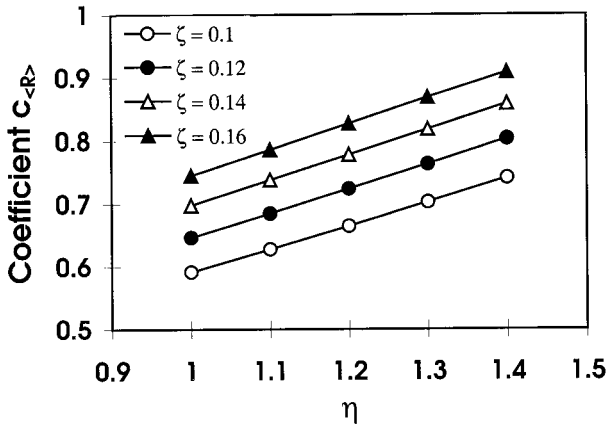

FIG. 7. Dependence of the coefficient $c_{\langle R\rangle}$ in σ_R–$\sigma_{\langle R\rangle}$ relation on the ACF parameters ζ and η.

we have to notice that $c_{\langle Q\rangle}$ represents the coefficient relating $\hat{\sigma}_R$ to $\hat{\sigma}_{\langle Q\rangle}$ when we use the sample data. In the following, we use A_{SRT} and $\langle R\rangle$; the former is used to obtain a statistical relation to estimate σ_R from the downlooking radar measurement, and the latter to compare with the theoretical calculation discussed above. The difference between $\langle R\rangle$ and A_{SRT} will be evaluated in section 4e. Figure 8 shows histograms of the coefficient $c_{A\mathrm{SRT}}$, which corresponds to $c_{\langle Q\rangle}$ in Eq. (23a), obtained with a linear regression of $\hat{\sigma}_R$ to $\hat{\sigma}_{A\mathrm{SRT}}$ and the correlation coefficient $r_{A\mathrm{SRT}}$ for the convective (types 1, 2, and 4) and stratiform (type 3) cases. For the convective cases, histograms are given for two cases: (case 1) the minimum rain rate of 0.1 mm h^{-1} and (case 2) the 5 mm h^{-1} rain rate to investigate the dependence of the regression result on rain rate since the NUBF correction is more important for higher rain rates. Note that the correlation coefficient is about 0.5 and slightly higher at the stratiform case and that in the convective case the coefficient $c_{A\mathrm{SRT}}$ is generally greater than it is in the stratiform case. As for the rain-rate dependence, case 2 gives slightly lower and more stable $c_{A\mathrm{SRT}}$ values than case 1.

Let us compare the result of the regression analysis between $\hat{\sigma}_R$ and $\hat{\sigma}_{\langle R\rangle}$ with the result obtained from the ACF parameters (Fig. 7). Figure 9 shows the histogram of $c_{\langle R\rangle}$ for 32 convective scenes. The mean value of 0.77 (case 2) compares fairly well with the calculation result (about 0.72) based on the ACF analysis shown in Fig. 7 with $\zeta = 0.135$ and $\eta = 1.13$. On the other hand, the result of case 1 (mean = 0.96) is significantly higher than the calculation result. Although the sample NSDs should underestimate the NSD of the parent PDF by the factor of $\sqrt{[(N-1)/N)]}$, where N is the number of data, the effect of this bias error, which causes a slight positive bias, would be rather small (about 2%) considering that both $\hat{\sigma}_R$ and $\hat{\sigma}_{\langle R\rangle}$ underestimate the parent PDF counterparts. Other possible causes of the discrepancy are (i) using the averaged 1D ACF may be a too simplified way to accurately predict the $\hat{\sigma}_R$–$\hat{\sigma}_{\langle R\rangle}$ relationship, and (ii) more rigorous treatment is necessary of the window effect to the rain-rate variability within a 4-km IFOV. The scattergram between $c_{\langle R\rangle}$ obtained from the $\hat{\sigma}_R$–$\hat{\sigma}_{\langle R\rangle}$ regression and the correlation distance r_c derived from ACF analyses is shown in Fig. 10, where r_c is defined as the distance at which the ACF is reduced to e^{-1}. It is found that there is a clear correlation between them, suggesting the possibility to relate the the ACF properties to the σ_R–$\sigma_{\langle R\rangle}$ relationship.

d. Lognormality of rain-rate PDF

To validate the assumption of lognormal distribution of rain rate within an FOV, the lognormality of rain rate for the spatial domain of several kilometers squares is examined by a χ^2 test. For this test, 49 rain-rate samples over a domain of 7 km by 7 km square are used, in which the χ^2 value is calculated only when at least 45 samples out of 49 are recognized as ''rainy.'' An example of the results is shown in Fig. 11, where χ^2 values are expressed as a cumulative distribution. In the distribution, χ^2 greater than about 10 is recognized as nonlognormal with the level of significance of 0.05 since we used an eight-category histogram to calculate the χ^2 value that should follow the χ^2 distribution for five degrees of freedom. Note that about 50% of the samples do not follow a lognormal distribution. We should note that a no-rain IFOV is not used to calculate a χ^2 value since there is an ambiguity in the treatment of ''zero'' rain rate. Figure 12 shows a summary of lognormality check of 42 rain scenes; the histogram of percentage of rain areas judged nonlognormal with 5% of significance from the χ^2 test. It is found that about 50% of the rain area may not be expressed as a lognormally distributed random field.

Including the zero rain rate in the χ^2 test should increases the χ^2 value, that is, nonlognormality. This suggests that the nonlognormality may be significant at storm edges and small isolated convective cells. In such cases, significant no-rain areas may exist within an IFOV, and we need to assume a delta-function PDF for the no-rain areas and another PDF for rainy areas. Such a mixed model was used in the NUBF study for microwave radiometer measurements (Graves 1993), but in the case of the spaceborne radar measurement, a model including a nonrainy region in an IFOV would be more difficult to apply because of the saturation of A_{SRT} due to the dominance of echo power from the nonrainy region (Kozu and Iguchi 1996). It is a next-step study subject to find alternative PDF that can better describe the rain-rate variability, to develop a method to detect a mixed rainy/nonrainy IFOV, and to apply a special procedure to such a mixed IFOV.

In spite of the above problems, we will assume the lognormal PDF in the simulation (described in the next section) to relate A_{SRT} to A_u because of its simplicity.

e. Radar measurable quantity other than A_{SRT}

In the above discussions and the investigations on rainfall characteristics, we have used A_{SRT} as the measurable quantity $\langle Q\rangle$. In cases where either rain attenuation is too small or normalized radar cross section (σ^0) of the surface varies considerably, we may not be able to use A_{SRT}. There may be other quantities that can be used to estimate PIA, however. One possibility is the PIA obtained from the sum of attenuations at each range gate estimated from the profile of Z factor including attenuation (Z_m) with a k–Z relation (A_{SU} or A_{ST}). The quantity $Z_m(r)$ is given by

$$Z_{m,i}(r) = \frac{1}{\sum_{j=1}^{n} w_j} \sum_{j=1}^{n} w_j Z_{j,i} \exp[-0.2 \ln 10 (r - r_0)\gamma Z_{j,i}^{\delta}], \tag{24}$$

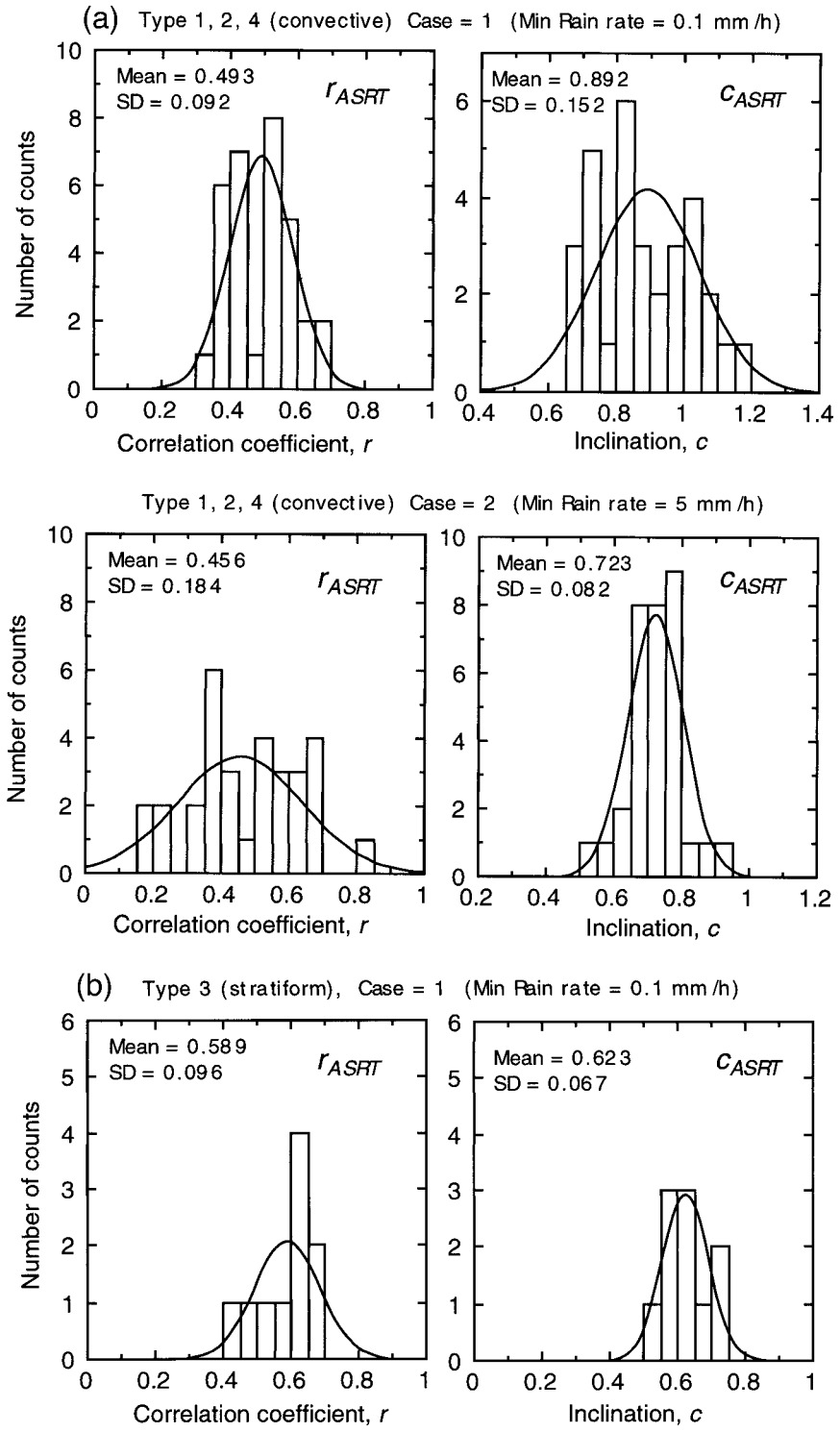

FIG. 8. (a) Histograms of correlation coefficient r_{ASRT} and the coefficient c_{ASRT} in $\hat{\sigma}_R$–$\hat{\sigma}_{ASRT}$ relation for rain types 1, 2, and 4 and for the minimum rain rate processed with 0.1 mm h^{-1} (case 1) and 5 mm h^{-1} (case 2). (b) The same as (a) except for type 3.

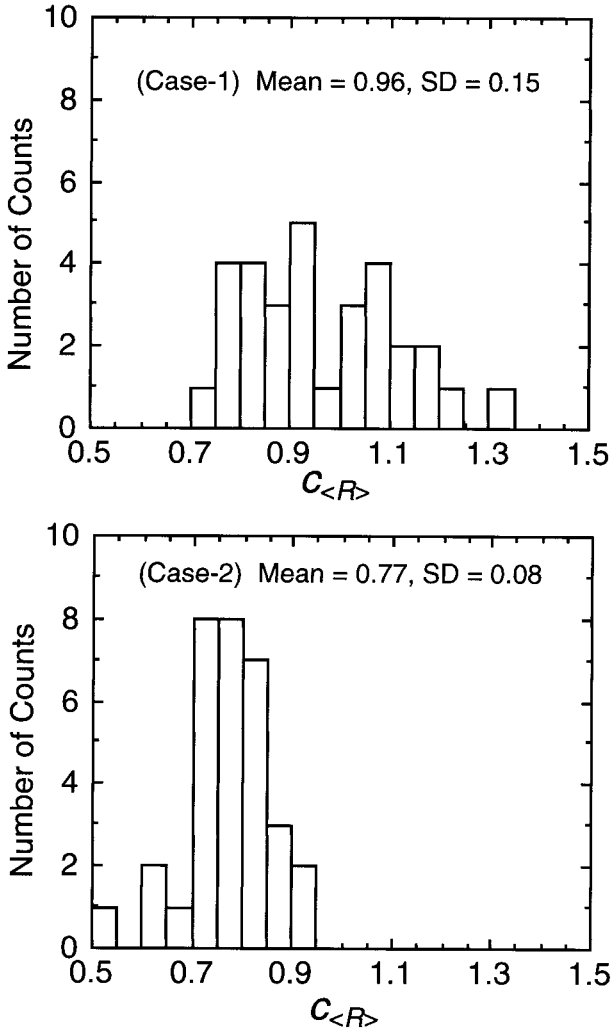

FIG. 9. Histogram of $c_{\langle R\rangle}$ for 32 convective scenes. Upper and lower panels show case 1 and case 2, respectively.

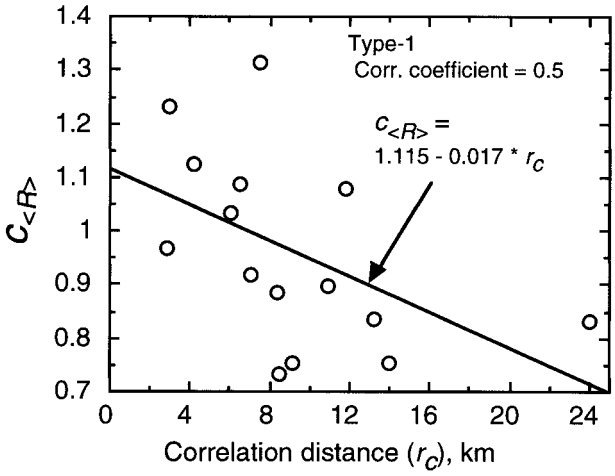

FIG. 10. Scattergram between $C_{\langle R\rangle}$ obtained from the $\hat{\sigma}_R$–$\hat{\sigma}_{\langle R\rangle}$ regression and the correlation distance r_c derived from the ACF analysis.

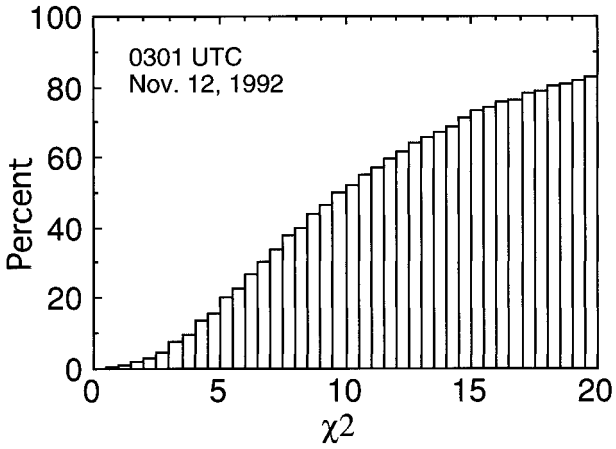

FIG. 11. An example of the χ^2 test results, where χ^2 values are expressed as a cumulative distribution.

where r_0 is the range at the storm top, and γ and δ are the coefficient and the exponent of the k–Z relation. PIA estimates (A_{SU} and A_{ST}) are expressed as follows:

$$A_{SU} = 4 \int_{r_0}^{r_0+L/2} \gamma Z_m(s)^\delta \, ds \tag{25}$$

$$A_{ST} = 2 \int_{r_0}^{r_0+L} \gamma Z_m(s)^\delta \, ds. \tag{26}$$

The difference between A_{SU} and A_{ST} is that the former uses Z_m factors at high altitudes only, so that it may

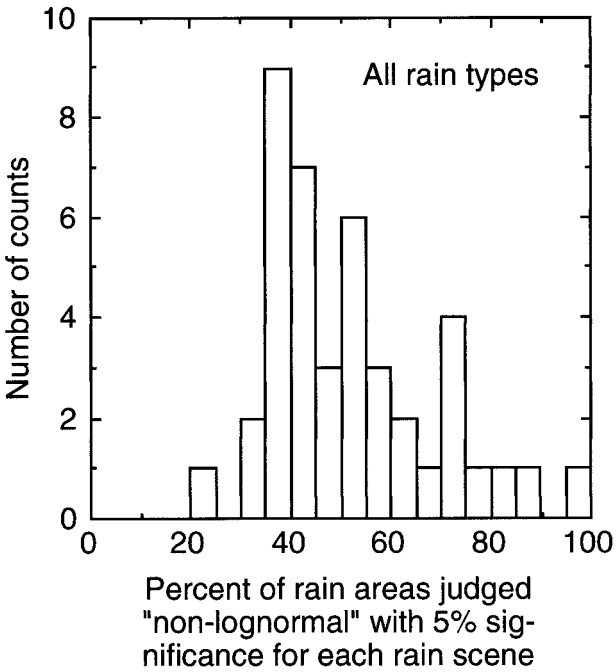

FIG. 12. A summary of lognormality check of 42 rain scenes; the histogram of percentage of rain areas judged nonlognormal with 5% of significance from the χ^2 test.

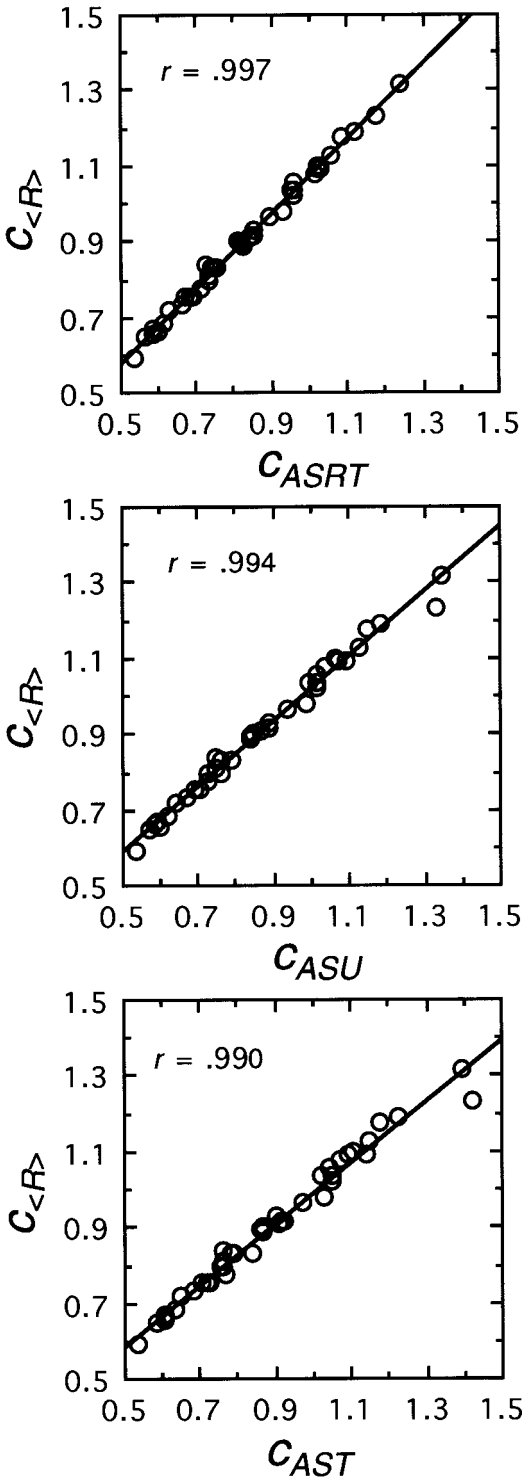

FIG. 13. Correlations between $c_{\langle Q\rangle}$'s obtained with the use of $\langle R\rangle$ and those obtained with the use of A_{SRT}, A_{SU}, or A_{ST}.

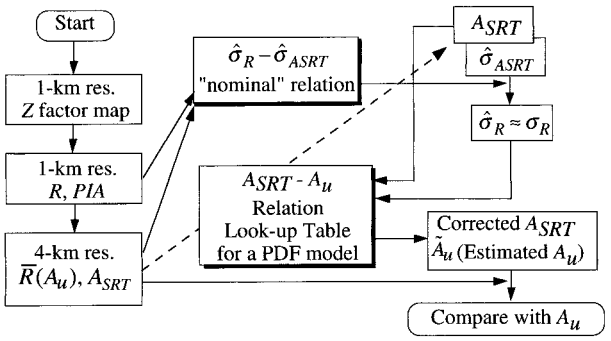

FIG. 14. Procedure of the simulation.

better be used for relatively intense rain cases than the latter, although it does not use rain information at rain bottom. Since A_{SU} and A_{ST} depend on the vertical structure of rain rate, the values obtained from the vertically uniform rain rate model assumed in this paper would not be the same as those from natural rain. Nevertheless, investigating the properties of these quantities under the vertically uniform rain would be useful for obtaining an approximate idea about the feasibility of using the Z_m profile alone. To test if we can use any quantity as $\langle Q\rangle$, depending on the rain and surface characteristics, correlations between $c_{\langle Q\rangle}$'s obtained with the use of $\langle R\rangle$ and those obtained with the use of A_{SRT}, A_{SU}, or A_{ST} are plotted in Fig. 13, suggesting the validity of using A_{SRT}, A_{SU}, and A_{ST} in place of $\langle R\rangle$.

In the standard Tropical Rainfall Measuring Mission (TRMM) precipitation algorithm (Iguchi et al. 1997), the quantity

$$\xi = -(10/\delta)\log\left[1 - 0.2\ln 10\epsilon\gamma\delta\int_{r_0}^{r_0+L} Z_m(s)^{\delta}\,ds\right] \quad (27)$$

is used. The factor ϵ is a parameter to be adjusted by using A_{SRT} or by assuming the Z-factor profile is vertically constant just above the surface. Although we do not test this type of PIA estimate, we can expect that ξ is similar to the quantities we have tested here since ξ is the same as A_{SRT} when SRT is reliable, and it should be generally a better estimate of PIA than A_{SU} or A_{ST}.

5. Simulation of the correction method

a. Simulation procedure

For a test of the NUBF correction method, simulations are performed using the same radar dataset as those used in the above analyses. The procedure of the simulation is depicted in Fig. 14. For the preparation of the simulation, we generate a lookup table (actually a set of regression lines of the result shown in Fig. 2, see Table 3) to obtain A_u from A_{SRT} and σ_R.

We first convert the 1-km spatial resolution Z-factor map to the corresponding rain rate and PIA. Next, we calculate the coarse-resolution rain rate and PIA of 4-km

TABLE 3. Coefficients a_0, a_1, and a_2 in $\log_{10}A_u = a_0 + a_1(\log_{10}A_{\mathrm{SRT}}) + a_2(\log_{10}A_{\mathrm{SRT}})^2$.

σ_R	a_0	a_1	a_2
0.2	0.0234	0.919	0.0784
0.4	0.0440	0.855	0.188
0.6	0.0553	0.849	0.276
0.8	0.0646	0.876	0.342
1.0	0.0750	0.919	0.391
1.2	0.0871	0.968	0.427
1.4	0.101	1.017	0.455

resolution by using Eqs. (17), (5′), and (19). At the same time, we calculate $\hat{\sigma}_R$ using Eq. (20) and $\hat{\sigma}_{\mathrm{ASRT}}$ using Eq. (21). The relationship between $\hat{\sigma}_R$ and $\hat{\sigma}_{\mathrm{ASRT}}$ [Eq. (23a) is also used for the relation between ''sample'' NSDs] has been established from a linear regression analysis of these quantities as we discussed in section 4c. In the current simulation, the mean c_{ASRT} for convective rain, case 2 (=0.723, see Fig. 8) is used for all types of rainfall.

With the above preparation, the simulation starts with an examination of the coarse-resolution radar measurement (A_{SRT}) of each IFOV. For a specific IFOV, we obtain A_{SRT} and $\hat{\sigma}_{\mathrm{ASRT}}$. The $\hat{\sigma}_{\mathrm{ASRT}}$ is then converted to $\hat{\sigma}_R$ using Eq. (23a). Here, A_{SRT} and the estimated $\hat{\sigma}_R$, which is treated as σ_R, are then input to the lookup table to obtain an estimate of A_u ($\tilde{A}_u$).

Since we use the same dataset for the simulation as that used to derive the $\hat{\sigma}_R$–$\hat{\sigma}_{\mathrm{ASRT}}$ relation, this simulation may not be a fully independent test of the method. It would still be useful and necessary to confirm the validity of this method with this type of simulation, however, because the coefficient c_{ASRT} to estimate $\hat{\sigma}_R$ from $\hat{\sigma}_{\mathrm{ASRT}}$ shows fairly wide variation when we look at the individual rain scene consisting of nine IFOVs, and the estimation of A_u from A_{SRT} and the estimated σ_R is a highly nonlinear, error-sensitive process. In addition, the validity of assuming the lognormal PDF can be tested with this simulation.

b. Simulation result

Following the procedure described above, simulations of the NUBF correction are performed; the results are shown in Figs. 15–18. In the figures, three scattergrams are compared for each rain type; one is the correlation between A_u and A_{SRT} (without correction), the second is that between A_u and $\tilde{A}_u$ (estimated A_u with the NUBF correction) using the estimated σ_R, and the third is the same as the second except that the ''true'' σ_R (strictly speaking, true $\hat{\sigma}_R$) is used. As shown in the figure, the NUBF-corrected results shown in panels b and c can improve the degree of underestimation of PIA, which is significant when no correction is applied. It is also clear, however, that over- and undercorrections are seen in some cases, particularly in types 1 and 2. In type 1, using the true σ_R significantly improves the tendency of overcorrection, suggesting the errors in estimating σ_R. On the other hand, in type 2, improvement by using the true σ_R is not significant, suggesting an improper PDF model causing an erroneous A_{SRT}–A_u relation. In the cases of types 3 and 4, the result of NUBF correction is better than types 1 and 2; in particular, the NUBF

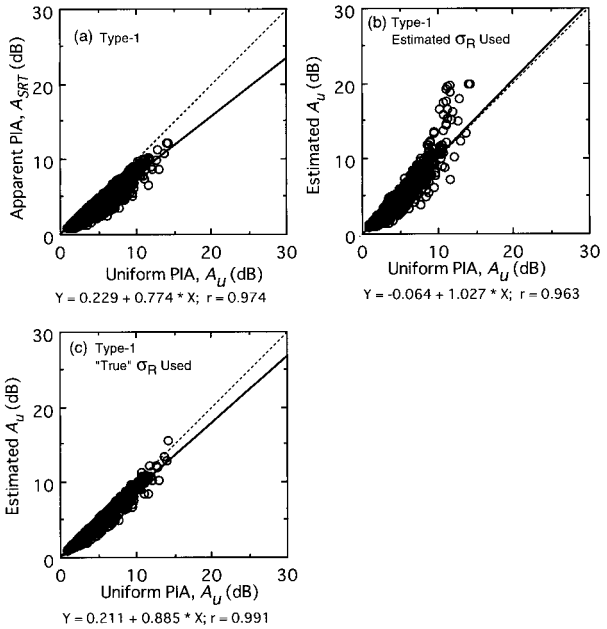

FIG. 15. Scattergrams (a) between A_u and A_{SRT} (without correction), (b) between A_u and $\tilde{A}_u$ (with NUBF correction) using the estimated σ_R, and (c) between A_u and $\tilde{A}_u$ (with NUBF correction) using the ''true'' σ_R for type 1 rainfall. Solid and dotted lines represent the linear regression result and the 1:1 correspondence line, respectively.

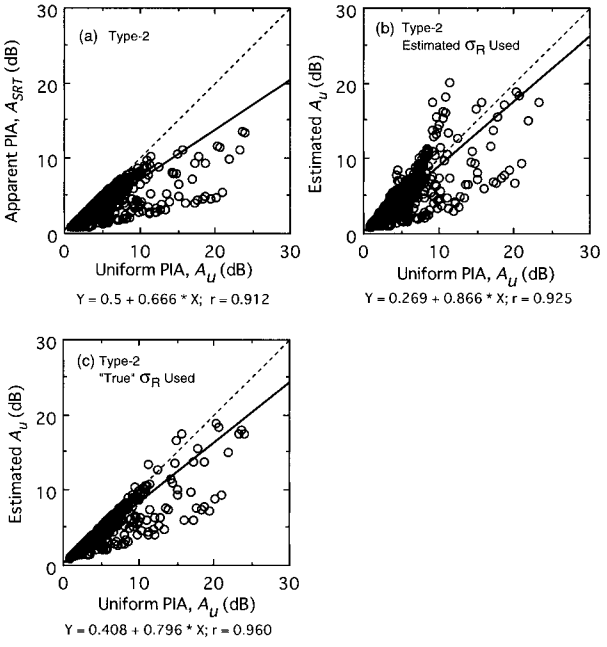

FIG. 16. The same as Fig. 15 except for type 2.

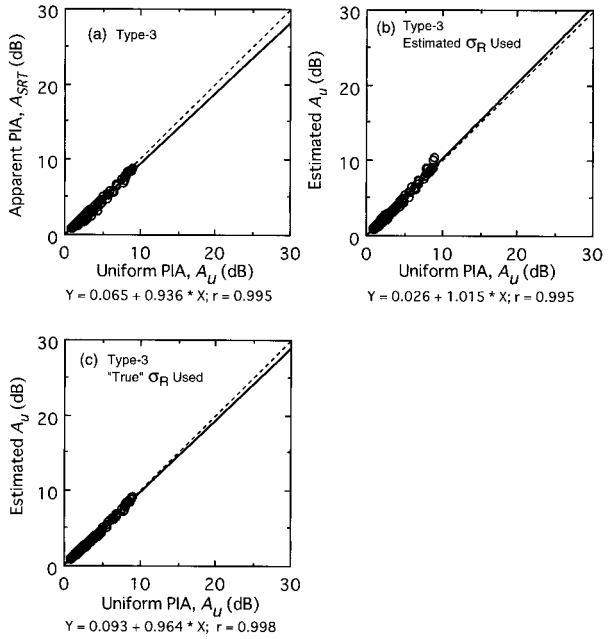

FIG. 17. The same as Fig. 15 except for type 3.

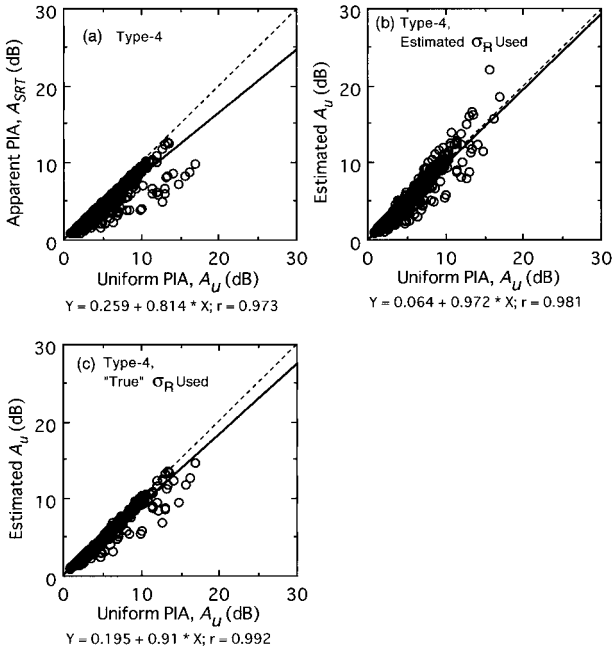

FIG. 18. The same as Fig. 15 except for type 4.

effect is very small in type 3, leading to stable NUBF corrections. From the above results it is clear that the ''instantaneous'' or ''IFOV-based'' NUBF correction can have considerable errors. Nevertheless, it can be concluded that the correction scheme tested here does work in general to reduce the significant negative bias errors due to the NUBF. Note that Durden et al. (1998) also obtained an encouraging result in testing an NUBF correction scheme using the data acquired by a KU-band airborne rain radar flown in the TOGA COARE field campaign.

The effectiveness of the NUBF correction can be seen more clearly from statistical comparisons. Figure 19 shows the ratio of cumulative probabilities of PIA for types 2 and 4. Each cumulative probability represents the percentage of occurrence of PIA that exceeds the given PIA value. In the figure, A_{SRT}/A_u and $\tilde{A}_u/A_u$ are plotted. Note that the NUBF correction can significantly improve the estimation accuracy of the cumulative distribution of PIA.

6. Conclusions

We have studied a method to make a correction of the path-integrated attenuation derived from spaceborne radar measurement for nonuniform beamfilling. The key to this method is the estimation of the finescale rain-rate variability within an IFOV (normalized standard deviation; σ_R) from the local statistics of a radar-measurable quantity ($\langle Q \rangle$), such as PIA derived from the surface reference technique. The estimated σ_R is then used to obtain a correction factor to estimate a rainfall quantity such as rain rate and PIA, which should be obtained when rain rate is uniform in the IFOV. In this paper, we have focused our attention to use SRT-derived PIA (A_{SRT}) to estimate the uniform PIA (A_u).

Statistical analyses have been made on spatial variabilities of these radar-measurable quantities using a shipborne radar dataset obtained from the TOGA COARE field campaign. The analyses include the spatial autocorrelation function, the finescale and coarse-scale rainfall variabilities, and lognormality of a rain-rate

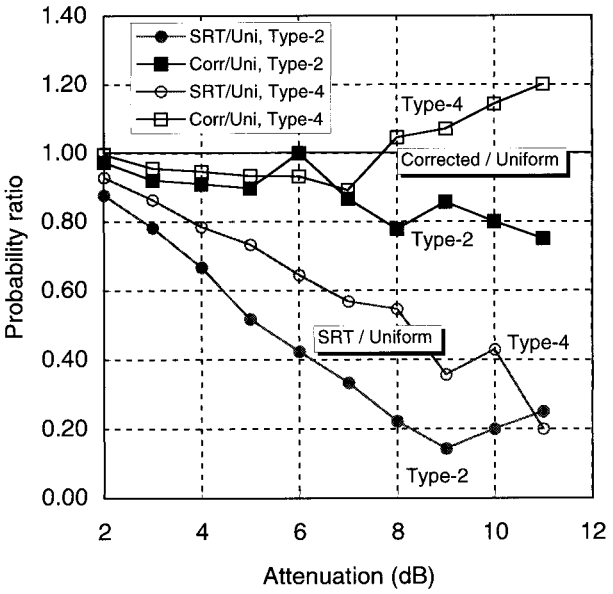

FIG. 19. Ratio of cumulative probabilities of PIA for type 2 and type 4.

PDF. There are reasonably good correlations between the coarse-scale variability of A_{SRT} and the finescale variability in an IFOV, and the regression coefficient (slope) of these two quantities is fairly stable. Based on the statistical analyses, the method is tested with a simulation using the same dataset. The test result indicates that this method is effective in reducing bias errors in the estimation of rain-rate statistics. It is also effective in making the NUBF correction for individual IFOV basis; in this case, however, one must account for the variability of local rainfall statistical characteristics, which may cause significant errors in estimating A_u. In the actual implementation of this method, therefore, some limitation on the magnitude of the correction factor (to retrieve A_u from A_{SRT}) or the magnitude of the estimated finescale variability (σ_R) may be needed to avoid a significant overcorrection for the NUBF.

Acknowledgments. We wish to thank Drs. C. Kummerow and D. A. Short of NASA/Goddard Space Flight Center (GSFC), Prof. K. Shimizu of Keio University, and Dr. N. Kashiwagi of the Institute of Statistical Mathematics for their valuable suggestions. Acknowledgment is also given to Mr. R. Okada, Remote Sensing Technology Center of Japan, who contributed to many of the statistical data analyses. The MIT radar data were kindly provided from the TOGA COARE project and TRMM Office, NASA/GSFC. This study was partly supported by National Space Development Agency of Japan (NASDA) under a joint research program between CRL and NASDA for the study of TRMM Precipitation Radar algorithms.

REFERENCES

Amayenc, P., M. Marzoug, and J. Testud, 1993: Analysis of cross-beam resolution effects in rainfall rate profile retrieval from a spaceborne radar. *IEEE Trans.,* **GE-31,** 417–425.

Durden, S. L. Z. S. Haddad, A. Kitiyakara, and F. K. Li, 1998: Effects of nonuniform beam filling on rainfall retrieval for the TRMM precipitation radar. *J. Atmos. Oceanic Technol.,* **15,** 635–646.

Graves, C. E., 1993: A model for the beam-filling effect associated with the microwave retrieval of rain. *J. Atmos. Oceanic Technol.,* **10,** 5–14.

Iguchi, T., T. Kozu, R. Meneghini, and K. Okamoto, 1997: Rain profiling algorithm for the TRMM precipitation radar. *Proc. International Geoscience and Remote Sensing Symp. (IGARSS'97),* Singapore, 1636–1638.

Kozu, T., and T. Iguchi, 1996: A preliminary study of non-uniform beam filling correction for spaceborne rain radar measurement. *IEICE Trans. Comm.,* **E79-B,** 763–769.

——, and ——, 1997: Correction: A preliminary study of nonuniform beam filling correction for spaceborne rain radar measurement. *IEICE Trans. Comm.,* **E80-B,** 989.

Kummerow, C., and L. Giglio, 1994: A passive microwave technique for estimating rainfall and vertical structure information from space. Part I: Algorithm description. *J. Appl. Meteor.,* **33,** 3–18.

Meneghini, R., and T. Kozu, 1990: *Spaceborne Weather Radar.* Artech House, 199 pp.

Morita, K., and I. Higuti, 1978: Statistical studies on rain attenuation and site diversity effect on Earth to satellite links in microwave and millimeter wavebands. *Trans. IEICE, Japan,* **E61,** 425–432.

Nakamura, K., 1991: Biases of rain retrieval algorithms for spaceborne radar caused by nonuniformity of rain. *J. Atmos. Oceanic Technol.,* **8,** 363–373.

Olsen, R. L., D. V. Rogers, and D. B. Hodge, 1978: The aR^b relationship in the calculation of rain attenuation. *IEEE Trans.,* **AP-26,** 318–329.

Short, D. A., P. A. Kucera, B. S. Ferrier, and O. W. Thiele, 1995: COARE IOP rainfall from shipborne radars: 1. Rain mapping algorithms. Preprints, *27th Conf. on Radar Meteorology,* Vail, CO, Amer. Meteor. Soc., 678–690.